Waste Management 147 (2022) 48–59

Contents lists available at ScienceDirect

Waste Management

journal homepage: www.elsevier.com/locate/wasman

Country report

Integration of steam gasification and catalytic reforming of lignocellulosic biomass as a strategy to improve syngas quality and pollutants removal

Eliana Quiroga [a], Bernay Cifuentes [b], Julia Moltó [c,d], Nuria Ortuño [c,d], Juan Conesa [c,d], Arantxa Davó-Quiñonero [e], Martha Cobo [a,*]

[a] Energy, Materials and Environment Laboratory, Universidad de La Sabana, Campus Universitario Puente del Común, Km. 7 Autopista Norte, Bogotá, Colombia
[b] Faculty of Engineering, Chemical Engineering, Universidad de La Salle, Carrera 2 # 10-70, Bogotá, Colombia
[c] Chemical Engineering Department, University of Alicante, Carretera de San Vicente del Raspeig, s/n, Alicante 03690, Spain
[d] University Institute of Chemical Process Engineering, University of Alicante, Carretera de San Vicente del Raspeig, s/n, Alicante 03690, Spain
[e] Department of Inorganic Chemistry, University of Alicante, Carretera de San Vicente del Raspeig, s/n, Alicante 03690, Spain

ARTICLE INFO

Keywords:
Dioxin elimination
Process integration
Steam reforming
Tar reforming
Thermochemical processes
Waste treatment

ABSTRACT

Residual biomass gasification is a promising route for the production of H_2-rich syngas. However, the simultaneous formation of pollutants such as light hydrocarbons (HCs), benzene, toluene and xylenes (BTEX), polycyclic aromatic hydrocarbons (PAHs), polychlorinated dibenzo-*p*-dioxins and dibenzofurans (PCDD/Fs) during gasification must be controlled. As a result, this study evaluated the effect of temperature and catalytic reforming over a Rh-Pt/CeO_2-SiO_2 catalyst during steam gasification of sugarcane residual biomass on syngas composition and pollutant removal. The above was carried out in a horizontal moving reactor, an Amberlite XAD-2 polyaromatic resin was used to collect the contaminants and characterization of the catalyst was performed. In this study, a concentration of up to 37 mol% of H_2, a yield of 23.1 g H_2 $kg^{-1}_{biomass}$, and a H_2/CO ratio $\geq$2 were achieved when gasification and reforming were integrated. In addition, the catalyst characterization showed that Rh-Pt/CeO_2-SiO_2 was not susceptible to sintering and favored the formation of hydroxyl groups that promoted CO oxidation, thereby increasing the H_2/CO ratio, as confirmed by *in-situ* diffuse reflectance infrared Fourier transform spectroscopy (DRIFTS). At 800 °C, where a high H_2 yield was obtained, 209 g Nm^{-3} of light HCs and BTEX, 10.9 g Nm^{-3} of PAHs, and 32.5 ng WHO-TEQ Nm^{-3} of PCDD/Fs were formed after gasification. Interestingly, after catalytic reforming, 62% of light HCs and BTEX, 60% of PAHs, and 94% of PCDD/Fs were removed, leading to cleaner syngas with properties that allow it to be used in a wide range of energy applications.

1. Introduction

Biomass conversion to syngas is key to the development of sustainable energy models and the production of valuable chemicals, thus effectively contributing toward the achievement of the Sustainable Development Goals (SDGs) (AlQattan et al., 2018). Thermochemical processes, especially gasification, are attractive routes for the production of syngas from lignocellulosic biomass, which is one of the most abundant renewable energy resources. Syngas obtained from gasification is mainly composed of hydrogen (H_2), carbon monoxide (CO), carbon dioxide (CO_2), methane (CH_4), and light hydrocarbons (HCs, C_2-C_8) (Shayan et al., 2018). H_2-rich syngas is desirable because of the high energy density of H_2 (122 MJ/kg), which is 2.7 times more than that of traditional fuels (Tan et al., 2020). Consequently, H_2-rich syngas obtained from gasification of lignocellulosic biomass could be a starting point for the establishment of sustainable energy models (Irfan et al., 2021; Shayan et al., 2018).

However, product distribution during gasification processes changes significantly due to the occurrence of several chemical reactions (Table 1) which depend on the operating conditions (e.g., gasifying agent and temperature) and the biomass source (Anniwaer et al., 2021). The use of steam as a gasifying agent (steam gasification) promotes H_2 production through reactions 1–5 in Table 1, while the use of air, oxygen, or pyrolysis conditions (without gasifying agent) mainly favors the formation of CH_4 (reaction 6 in Table 1) and CO (reactions 8–10 in Table 1) (Quiroga et al., 2020). However, an excess of steam would demand high energy consumption to heat water (Wu et al., 2014). Thus, a steam-to-biomass weight ratio (S/B) between 0.5 and 2.5 is suggested

* Corresponding author.
E-mail address: martha.cobo@unisabana.edu.co (M. Cobo).

https://doi.org/10.1016/j.wasman.2022.05.012
Received 14 January 2022; Received in revised form 18 April 2022; Accepted 14 May 2022
Available online 24 May 2022

Table 1
Reactions involved in biomass gasification and the catalytic reforming of syngas (He et al., 2020; Siddik Aydin et al., 2019).

Gasification and reforming reactions			Eq.
$Biomass_{wet} \rightarrow Biomass_{dry} + H_2O$		Drying	(1)
$Biomass_{dry} \rightarrow C + Tar + gas$		Gasification	(2)
$CH_4 + H_2O \leftrightarrow CO + 3H_2$	+207 kJ mol^{-1}	Steam Reforming of methane (SRM)	(3)
$C + H_2O \leftrightarrow CO + H_2$	+131 kJ mol^{-1}	Water-gas	(4)
$CO + H_2O \leftrightarrow CO_2 + H_2$	−41.1 kJ mol^{-1}	Water-gas shift (WGS)	(5)
$CO + 3H_2 \leftrightarrow CH_4 + H_2O$	+103 kJ mol^{-1}	Methanation	(6)
$C + O_2 \rightarrow CO_2$	−283 kJ mol^{-1}	Combustion	(7)
$C + CO_2 \leftrightarrow 2CO$	+172 kJ mol^{-1}	Boudouard	(8)
$CH_4 + 0.5\,O_2 \leftrightarrow CO + 2H_2$	−36 kJ mol^{-1}	Partial oxidation of methane	(9)
$CH_4 + CO_2 \leftrightarrow 2CO + 2H_2$	+248 kJ mol^{-1}	Dry reforming of methane (DRM)	(10)
Light HC and tar decomposition reactions			
$C_nH_{2n+2} \rightarrow C_{n-1}H_{2(n-1)} + CH_4$		Cracking	(11)
$C_nH_m + nH_2O \rightarrow nCO + (n + 0.5m)H_2$		Steam reforming*	(12)
$C_nH_m + nCO_2 \rightarrow 2nCO + (0.5m)H_2$		Dry reforming*	(13)

*C_nH_m represents light HC and tar components.

to increase the syngas quality in terms of the H_2 concentration and to reduce the energy demand of the process (Hu et al., 2019; Lin and Weng, 2017).

On the other hand, temperature influences H_2 concentration and gas yield. For instance, Yan et al. studied the effect of temperature on the hydrothermal gasification of organic waste, results showed that H_2 selectivity and the lower heating value (LHV) increase (68.53% to 96.09% and 4.15 to 12.17 MJ Nm^{-3}, respectively) with an increase in temperature from 420 to 500 °C (Yan et al., 2020). Hwang et al. reported that the H_2 concentration and gas yield obtained from steam gasification of wood waste were four times higher when the temperature was raised from 500 to 700 °C, yielding 20 vol% of H_2 in the syngas and a gas yield of 1.24 Nm^3 kg^{-1} (Hwang et al., 2014). These authors attributed the increase in gasification efficiency to the occurrence of steam reforming of CH_4 (SRM, Eq. 3 in Table 1) and the water–gas reaction (Eq. 4 in Table 1), which is favored by temperature (Hwang et al., 2014). Similarly, Anniwaer et al. indicated that increasing the temperature from 750 °C to 850 °C favors SRM, thereby increasing the H_2 content from 35 to 67 vol%. Thus, the temperature improves the H_2 concentration in syngas obtained from gasification (Anniwaer et al., 2021). Nonetheless, temperature selection for gasification may involve other aspects, including energy and environmental considerations.

Despite the effectiveness of steam gasification in the production of syngas, the formation of solid (char) and liquid (condensables and tar) phases are also expected due to cracking reactions (Eq. 11 in Table 1) and coke formation (Eq. 2, and reverse 8 in Table 1) (Hiblot et al., 2016). Char, condensables, and tar could affect H_2 production and imply high maintenance costs for equipment (Katsaros et al., 2019; Tan et al., 2020). Tar is composed of organic compounds known as polycyclic aromatic hydrocarbons (PAHs) (i.e., naphthalene, acenaphthylene, and acenaphthene, among others), excluding light HCs and benzene, toluene and xylenes (BTEX) (Hernández et al., 2013; Nguyen et al., 2018). PAHs can condense at low temperatures (~100 °C) and low concentrations (~1 mg Nm^{-3}) (Valderrama Rios et al., 2018), resulting in serious environmental problems (Moltó et al., 2020). In addition, other compounds such as polychlorinated dibenzo-*p*-dioxins and dibenzofurans (PCDD/Fs) (Edo et al., 2018; Palmer et al., 2021), which are persistent environmental pollutants can be released. PCDD/Fs can be formed during thermal conversion processes due to the formation of intermediaries such as C—Cl containing HCs (Conesa et al., 2020; Zhang et al., 2018b). Therefore, mitigating the formation of these undesirable phases (solid, liquid and C—Cl containing HCs) is a critical to ensuring the sustainability of steam gasification.

Several alternatives have been proposed to reduce the formation of solid and liquid phases and C—Cl containing HCs during gasification. Catalytic gasification, in which catalysts are mixed with biomass in a single fluidized bed reactor, is an effective way to reduce tar formation during thermochemical processes (Fremaux et al., 2015; Wu and Williams, 2010). Nevertheless, the formation of coke, even in small quantities, leads to the rapid deactivation of the catalysts, thereby demanding frequent replacement of the catalyst, and increasing operating costs (Liu et al., 2019a). Thus, downstream treatments of the outlet syngas from the gasification process have been receiving more attention in recent years.

Recently, Hu et al. (Hu et al., 2019) studied the steam gasification of corn straw followed by catalytic steam reforming of syngas with a Ni/γ-Al_2O_3 catalyst, and reported that the integration of both processes (i.e., gasification followed by catalytic reforming) results in an increase of H_2 concentration in the syngas up to 1.7 times of that obtained from the steam gasification (28.4 mol% of H_2). Zhang et al. evaluated the cleaning of syngas obtained from gasification of municipal solid waste via catalytic reforming with Ni-based catalysts and reported that the tar concentration in syngas decreased by approximately 50% after going through the reformer unit (Zhang et al., 2018a). Also, catalytic processes have been shown to be a promising option to inhibit the formation of PCDD/Fs in syngas, for instance, Kawamoto et al. (Kawamoto et al., 2009) and Weiland et al. (Weiland et al., 2021) reported the effect of steam gasification and temperature on the inhibition of PCDD/F formation and showed that at temperatures >700 °C decomposition of PCDD/Fs during biomass gasification increases to almost 100% (Kawamoto et al., 2009). Consequently, carrying out a catalytic reforming step after gasification could be a promising strategy for the production of H_2-rich syngas, the protection of the catalyst, and the reduction of pollutants present in tar.

Most of the catalysts that are used for the reforming of syngas are Ni-based because of their high activity and low cost (Irfan et al., 2021; Vita et al., 2014). However, Ni catalysts are susceptible to deactivation (by the impurities present in the syngas) and sintering due to the high temperatures (>600 °C) at which gasification is carried out (Zhang et al., 2018a), thereby losing activity and selectivity. Consequently, new approaches such as the use of other transition metals, alkali catalysts, zeolites, active carbon, minerals, and low-load noble-metal-based catalysts have been studied (Izquierdo et al., 2014, 2017; Liu et al., 2019a). Asadullah et al. compared Rh/CeO_2/SiO_2 and dolomite (a mineral containing $CaMg(CO_3)_2$) as catalysts for the reforming of char and tar obtained from cedar wood biomass gasification (Asadullah et al., 2002). They reported that at 700 °C, the Rh/CeO_2/SiO_2 catalyst favored the production of syngas with a H_2/CO ratio four times higher than that of dolomite due to the stability, selectivity, and resistance of noble metals under gasification conditions (Asadullah et al., 2002). In addition, in a recent study (Quiroga et al., 2020), we evaluated the thermal degradation of sugarcane residual biomass over a Rh-Pt/CeO_2-SiO_2 catalyst for syngas production, and found that the Rh-Pt/CeO_2-SiO_2 catalyst promotes reforming reactions (Eqs. 5–7 and 11 in Table 1) at temperatures above 550 °C, thereby increasing the H_2 concentration in the syngas. We also identified that the Rh-Pt/CeO_2-SiO_2 catalyst promotes the degradation of C2 and C3 species (Quiroga et al., 2020), which could be a positive feature for the removal of tar and other pollutants during gasification. This catalyst (Rh-Pt/CeO_2-SiO_2) has also been evaluated in other reforming processes, where it has shown resistance to impurities in the inlet stream and led to the production of H_2-rich syngas for energy applications without evidence of deactivation (Cifuentes et al., 2021).

Despite the effectiveness of this catalyst in reforming reactions, it has not been evaluated for the reforming of syngas obtained directly from a gasifier.

In this study, the effectiveness of catalytic reforming over a Rh-Pt/CeO_2-SiO_2 catalyst as a downstream treatment method of syngas obtained from the gasification of sugarcane residual biomass was evaluated. This evaluation involved an assessment of the change in product distribution between a simple gasification process and a gasification system followed by a catalytic treatment. Furthermore, the emission of pollutants, such as light HCs, PAHs, and PCCD/Fs, commonly formed during biomass thermochemical processes, was considered a point of comparison between the two processes (i.e., between gasification and gasification followed by catalytic reforming). Characterization tests were also performed to establish how the properties of Rh-Pt/CeO_2-SiO_2 influence its performance during syngas reforming.

2. Experimental

2.1. Collection and selection of residual biomass samples

Residual liquid sugarcane press-mud collected from Tolima, Colombia, was used as a lignocellulosic biomass resource. Details of the sample collection and characterization can be found in Supplementary Material.

2.2. Catalyst preparation and characterization

The synthesis of the Rh-Pt/CeO_2-SiO_2 catalyst was carried out according to the methodology reported by Cifuentes et al. (Cifuentes et al., 2016). An aqueous solution of $Ce(NO_3)_3{\cdot}6H_2O$ (Merck, Germany) was slowly added to SiO_2 (Merck, Germany) with constant stirring to achieve a Ce/Si molar ratio of 2. Then, the mixture was dried in a furnace for 24 h at 80 °C and calcined in a muffle furnace at 500 °C (5 °C min^{-1}) for 4 h to obtain the CeO_2-SiO_2 support. Subsequently, Rh (0.4 wt%) and Pt (0.4 wt%) were loaded onto the CeO_2-SiO_2 support by the incipient wetness co-impregnation method, using solutions of $RhCl_3{\cdot}H_2O$ (Merck, Germany) and $H_2PtCl_6{\cdot}6H_2O$ (Merck, Germany) in deionized water (DI) as precursors. The mixture was dried in a furnace at 80 °C for 24 h, calcined in a muffle at 700 °C (5 °C min^{-1}) for 2 h, and reduced with 8% H_2/He (200 mL min^{-1}) at 700 °C. Finally, the powder obtained was sieved through an 80-mesh sieve.

The obtained samples were characterized by different techniques. Morphology of samples was evaluated by high-resolution transmission electron microscopy (HR-TEM). For this, samples were ultrasonically dispersed in ethanol and placed on a copper grid coated with a carbon film. The micrographs obtained from HR-TEM were employed to measure the diameter of the active metal particles using ImageJ software. At least 150 particles were counted per sample. The average surface-area-weighted diameter of the active metal particles (Rh and Pt) was calculated according to Eq. (14) (Cifuentes et al., 2016).

$$\overline{d_s} = \frac{\sum_i n_i d_i^3}{\sum_i n_i d_i^2} \tag{14}$$

where n_i is the number of particles and d_i is the particle diameter.

Structure of samples was studied by X-ray diffraction (XRD). For this, XRD spectra were recorded at 2θ with a step size of 0.05°, and a step time of 3 s, and the deviation from the peak position was ≤0.002°. The crystal size of CeO_2 was calculated using the Scherrer equation (Eq. (15)) (Cavusoglu et al., 2015).

$$d_{hkl} = \frac{0,089\lambda}{\beta Cos(\theta)} \tag{15}$$

where β is the width of half the height of the XRD peak in radians, and θ is the angle between the incident and diffracted X-ray beam.

X-ray photoelectron spectroscopy (XPS) was performed on the aged samples in order to see the oxidation states of the metals present in the catalysts. Spectra of aged catalysts were obtained using an electron spectrometer (K-ALPHA, Thermo Scientific) with a twin anode radiation source in the Al-Kα (1486.6 eV) constant energy analysis mode and an energy flow of 50 eV. The C 1s line was set at 284.6 eV. The binding energy (BE) values were obtained with a precision of 0.2 eV.

in-situ diffuse reflectance infrared Fourier transform spectroscopy (DRIFTS) were performed using 40 mg of Rh-Pt/CeO_2-SiO_2 catalyst placed in a quartz cell, reduced *in situ* using 8% H_2/N_2 at 500 °C for 1 h, and then flushed with Ar (120 mL min^{-1}) for 10 min. Tests were carried out from 25 to 500 °C, in the range of 4000 to 1000 cm^{-1}, with an average of 32 scans min^{-1} and a resolution of 4 cm^{-1}. Once the test temperature was reached, the catalyst sample was flushed with test gases (10% CH_4/Ar, 5% CO/Ar, 5% CO_2/Ar, or a mixture of these gases) at 120 mL min^{-1} for 10 min (adsorption step). The catalyst was then flushed with Ar (120 mL min^{-1}) for 10 min (desorption step). Finally, the system was cooled, and the procedure was repeated. Each spectrum was obtained by subtracting the background of the reduced samples.

2.3. Steam gasification

Steam gasification of sugarcane residual biomass was tested between 600 and 800 °C in a moving horizontal reaction system, for a detailed diagram of the experimental set-up, see Fig. 1. The system consisted of an arrangement of two quartz containers in line with a quartz tube (7 cm in length and an internal diameter of 0.5 cm), which was heated using an electric furnace and moved horizontally at a constant speed (0.1 mm s^{-1}) using an SA5H-500 actuator (IAI, USA). A sample mass of 1.0 g of sugarcane residual biomass was distributed uniformly in the quartz containers, achieving a constant feed rate of 0.049 g min^{-1}. Steam was supplied by bubbling water with a controlled flow of N_2 (100 mL min^{-1}) as the carrier gas to ensure an S/B ratio of 2.2 and a steam flow rate of 0.139 mL min^{-1}. A uniform temperature of 90 °C was maintained in the bubbler using a silicone resistor with temperature sensors and a power controller.

Condensable compounds in the outlet stream of the reactor were collected in an Amberlite XAD-2 polyaromatic resin (Supelco, Bellefonte, USA), which was operated at 130 °C. Finally, the syngas produced was cooled and collected in 5 L Tedlar bags (Restek, Bellefonte, PA, USA). The collected steam gasification samples were labeled as "G-X", where G refers to steam gasification and X represents the temperature at which the test was carried out.

2.4. Catalytic reforming

Catalytic reforming of the syngas obtained from steam gasification of sugarcane residual biomass was evaluated at 600, 700, and 800 °C in the reaction system described above (Fig. 1). The catalytic bed consisted of 0.2 g of Rh-Pt/CeO_2-SiO_2 catalyst distributed in two quartz wool plugs, which were placed in the reactor, 40 mm from the last container, ensuring a gas hourly space velocity of 44 829 h^{-1}. The sampling of the products obtained in the integrated system was the same as described in section 2.4 for the steam gasification tests. For all the experiments, the plug flow reactor condition was achieved by eliminating back mixing and channeling ensuring a ratio between the catalyst bed height and catalyst particle size (L/Dp) and a ratio between the reactor internal diameter and catalyst particle size (D/Dp) higher than 60 (Sahoo et al., 2007). Samples of spent catalysts and product samples obtained were labeled as "GR-X", where GR refers to the coupling of steam gasification and catalytic reforming processes, and X represents the temperature at which each test was carried out.

The syngas samples collected in Tedlar bags were analyzed using gas chromatography (GC). The production of H_2, CH_4, CO, and CO_2 was measured in a 7820A unit (Agilent, CA, USA) equipped with a Haye Sep Q 80/100 column and a Molecular Sieve 5A 80/100 column (Teknokroma, BCN, Spain) connected to a thermal conductivity detector. Prior to

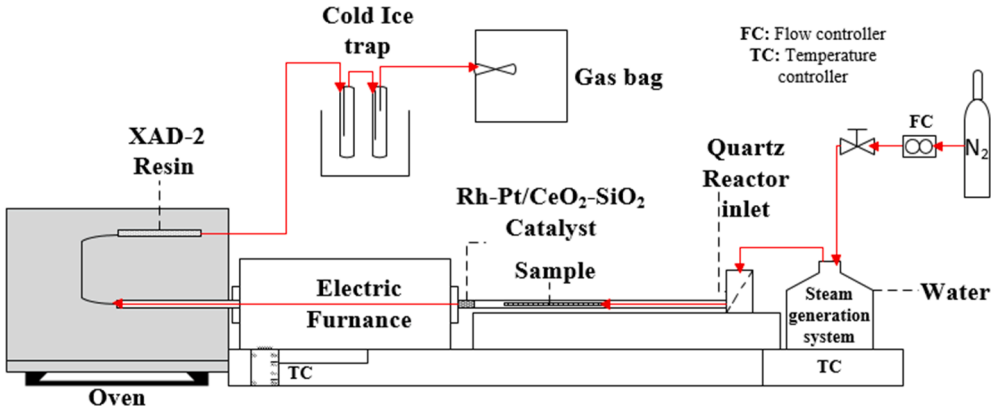

Fig. 1. Diagram of the laboratory-scale moving horizontal tubular reactor used in the steam gasification experiments.

the identification and quantification of the analytes in the experimental samples, an external calibration was carried out using high-purity standards for each gas.

Then, the S/B ratio, biomass conversion, gas yield, and LHV were calculated according to Eqs. (16)–(19).

$$S/B = m_{H_2O}/m_{biomass_{db}} \tag{16}$$

$$Biomass\ \ conversion[\%] = (1 - M_{char}/M_{biomass})*100 \tag{17}$$

$$Carbon\ \ conversion[\%] = \left(1 - \frac{M_{carbon_{char}}}{M_{carbon_{biomass}}}\right)*100 \tag{18}$$

$$Dry\ \ gas\ \ yield[Nm^3 kg^{-1}_{biomass}] = V_t/M_{biomass} \tag{19}$$

$$LHV\ \ yield\left[MJkg^{-1}_{biomass}\right] = Gasyield(12.6C_{CO} + 10.80C_{H_2} + 35.8C_{CH_4})/M_{biomass} \tag{20}$$

where m_{H_2O} is the mass flow (g min^{-1}) of H_2O in the inlet stream of the system, $m_{biomass_{db}}$ is the mass flow (g min^{-1}) of biomass on a dry basis in the inlet stream of the system, M_{char} is the mass (kg) of char, $M_{biomass}$ is the initial mass (kg) of biomass on a dry basis, $M_{carbon_{char}}$ is the mass of carbon contained in the char, $M_{carbon_{biomass}}$ is the mass of carbon contained in the initial biomass on a dry basis, V_t is the total volume (m^3) of the produced syngas under normal conditions, and C is the gas concentration in vol%.

2.5. Pollutant quantification

Light HCs and BTEX compounds were analyzed in a GC-17A unit (Shimadzu, Kyoto, Japan) equipped with an alumina KCl plot capillary column (Sigma-Aldrich, MO, USA) connected to a flame ionization detector. The identification and quantification of these compounds was carried out by external standard calibration by comparing the retention times of the analytes with those obtained from the calibration curve. The values reported are the average of triplicate injections of the samples.

The quantification of PAHs was carried out following the US EPA 8270D method (US EPA, 2018). Before each experiment, internal standards were added to the XAD-2 resin. The 16 priority PAH deuterated standards were provided by Dr. Ehrenstorfer-Schäfers (Augsburg, Germany). Before the analysis, the resin obtained at the end of each run was extracted using an ASE-100 (Dionex, Thermo Fisher Scientific, California, USA). PCDD/F formation was analyzed only for the experiments at 700 and 800 °C by collecting them in the XAD-2 resin following a standard methodology developed in our lab (Conesa et al., 2020; Gandon-Ros et al., 2021), detailed quantification methods and procedures can be found in Supplementary Material. For all experiments, laboratory blanks (without sample) were performed before each test under the same conditions as the test runs. The reaction conditions, processed Excel data of activity, and characterization tests can be observed in detail and downloaded from [dataset] (Quiroga et al., 2021).

3. Results and discussion

3.1. Biomass steam gasification

Table 2 shows the product distribution and gas yields obtained from the steam gasification of sugarcane residual biomass with a S/B ratio of 2.2 for all the experiments. High temperatures favor biomass carbon conversion (Huang et al., 2013), thereby improving steam gasification performance; thus, at 800 °C, high conversions of sugarcane residual biomass (up to 82%) and carbon (up to 82%) were achieved (Table 2). The gas yields of the main species (H_2, CO, CH_4, and CO_2) also increased with temperature due to the promotion of gasification (Eq. 2 in Table 1) and reforming reactions (Eqs. 3–4 and 12 in Table 1), thereby reducing the formation of condensable compounds (Fremaux et al., 2015). Therefore, the increase in both biomass conversion and H_2 yield with temperature contributed to the production of syngas with a H_2 concentration of 19.5 mol% at 800 °C.

Syngas applications depend on both H_2 concentration and gas composition in terms of H_2/CO, H_2/CH_4, and CO_2/CO molar ratios (Lalsare et al., 2019; Terrell and Theegala, 2019). Table 2 shows that the H_2/CO ratio increases with temperature to 0.9 at 800 °C, owing to the occurrence of steam reforming reactions (Eqs. 3, 4, and 12 in Table 1). However, this H_2/CO ratio is still low for use in energy applications, even for CO-tolerant H_2 fuel cells, because a high (>1) H_2/CO molar ratio is required (Cifuentes et al., 2021). Similarly, the H_2/CH_4 molar ratio is used to establish the syngas energy potential because H_2 has a higher energy density than CH_4 (Hiblot et al., 2016; Terrell and Theegala, 2019). The endothermic SRM reaction (Eq. 3 in Table 1) could contribute to an increase in the H_2/CH_4 ratio with temperature (Fremaux et al., 2015), as shown in Table 2. Thus, comparable amounts of H_2 and CH_4 (H_2/CH_4 ratio of 1) were obtained at 800 °C (Table 2) during the steam gasification process, resulting in a high LHV (4.4 MJ $kg^{-1}_{biomass}$, Table 2) and dry gas value (0.4 Nm^3 $kg^{-1}_{biomass}$, Table 2).

Furthermore, the CO_2/CO molar ratio was used to deduce the main chemical reactions involved in the thermochemical processes. CO is mainly formed by SRM, water–gas, Boudouard, and tar steam reforming reactions (Eqs. 3, 4, 8, and 12 in Table 1), while most of the CO_2 comes from the WGS and combustion reactions (Eqs. 5 and 7, respectively, in Table 1). CO_2/CO ratio in the syngas (Table 2) slightly decreases with temperature from 1.9 at 600 °C to 1.3 at 800 °C. This behavior can be ascribed to the endothermic reverse WGS reaction (Eq. 5 in Table 1), which is favored at high temperatures (Yu et al., 2020).

Therefore, steam gasification at high temperatures is preferred, to increase biomass conversion and H_2 concentration in the syngas. Nonetheless, the H_2/CO ratio of the syngas produced is still low for its practical use in energy applications. To overcome this issue, catalytic

Table 2
Product distribution in syngas during steam gasification and after catalytic reforming at S/B of 2.2. Mean values ± standard deviation of the measurements are shown.

Aspect	Outlet stream					
	Gasification			Catalytic reforming		
	G-600	G-700	G-800	GR-600	GR-700	GR-800
Biomass conversion (%)	79.4 ± 0.8	80.8 ± 0.6	82.7 ± 1.5	79.4 ± 0.3	80.8 ± 0.1	82.1 ± 0.3
Gas yield (g compound kg^{-1} of biomass)						
H_2	0.8 ± 0.013	1.5 ± 0.2	7.1 ± 0.12	5.4 ± 0.3	10.4 ± 0.8	18.8 ± 0.07
CO	34 ± 2	54 ± 4	117.6 ± 3	30.1 ± 0.6	54.5 ± 4	129.0 ± 0.6
CH_4	12.3 ± 0.09	30.4 ± 0.2	58.9 ± 9	12.4 ± 0.04	30.5 ± 0.4	44.4 ± 0.3
CO_2	103 ± 6	112 ± 6	234.6 ± 8	203.6 ± 1.3	297 ± 5.4	369 ± 3
Light HCs and BTEX	24.9 ± 0.4	61.5 ± 0.4	76.7 ± 3	23.7 ± 0.7	51.5 ± 0.7	28.2 ± 0.2
H_2/CO	0.3 ± 0.02	0.4 ± 0.03	0.9 ± 0.02	2.5 ± 0.09	2.7 ± 0.11	2.1 ± 0.0
H_2/CH_4	0.5 ± 0.02	0.4 ± 0.03	1.0 ± 0.1	3.5 ± 0.2	2.7 ± 0.2	4.1 ± 0.02
CO_2/CO	1.9 ± 0.03	1.3 ± 0.1	1.3 ± 0.01	4.3 ± 0.1	3.5 ± 0.2	1.8 ± 0.01
LHV of gas [MJ kg^{-1} of biomass]	1.3 ± 0.03	2.1 ± 0.1	4.4 ± 0.3	1.9 ± 0.05	3.4 ± 0.1	7.0 ± 0.02
LHV of gas [MJ Nm^{-3}]	9.0 ± 0.1	12.2 ± 0.1	12.2 ± 0.7	7.3 ± 0.1	8.8 ± 0.1	9.6 ± 0.03
Dry Gas yield [Nm^3 kg^{-1} of biomass]	0.2 ± 0.003	0.2 ± 0.0	0.4 ± 0.01	0.3 ± 0.0	0.4 ± 0.01	0.7 ± 0.0
Gas composition (mol%)						
H_2	7.4 ± 0.4	8.8 ± 0.6	19.5 ± 0.6	28.0 ± 1.1	30.6 ± 1.1	37.3 ± 0.07
CO	23.3 ± 0.3	22.9 ± 1.4	22.9 ± 0.9	11.1 ± 0.09	11.5 ± 0.5	18.2 ± 0.006
CH_4	14.7 ± 0.05	23.4 ± 0.4	20 ± 2	8.0 ± 0.11	11.3 ± 0.3	9.0 ± 0.05
CO_2	45.0 ± 0.4	30.3 ± 1.1	29.1 ± 1.0	47.8 ± 1.0	40.0 ± 1.0	33.2 ± 0.13
Light HCs and BTEX	9.5 ± 0.07	14.5 ± 0.2	8.3 ± 0.4	5.1 ± 0.07	6.6 ± 0.2	2.3 ± 0.002

reforming as a downstream treatment of the syngas derived from gasification was studied, and the findings were compared with those of steam gasification (*vide infra*).

3.2. Steam gasification followed by catalytic reforming

The product distribution and gas yields for the integrated system (gasification followed by catalytic reforming) are presented in Table 2. The results show that after catalytic reforming, H_2 and CO_2 yields clearly increase, while CH_4, CO, light HC, and BTEX yields either decreased or were maintained at similar levels, compared to those for steam gasification. Thus, the use of catalytic reforming as a downstream treatment method for syngas increases H_2 concentration 1.9 times, ensuring the production of a syngas with 37.3 mol% H_2 at 800 °C. Nevertheless, the obtained H_2 concentrations (- 30 vol%) were below the levels of the literature reports (40 vol% H_2) (Hu et al., 2015; Irfan et al., 2021; Kawamoto et al., 2009). Lower H_2 concentrations can be related to the low moisture content (<3 wt%) of the residual biomass used in this study. Moisture contents of about 10 wt% increases the total steam during gasification (Hu et al., 2015), favoring SRM, WGS and SR reactions (Eqs 3, 5 and 12 in Table 1) by Le Chatelier's principle.

Table 2 also shows that the H_2/CH_4 ratio increases after catalytic reforming, reaching a value of 4.1 at 800 °C. Studies have proven that the SRM and DRM reactions (Eqs. 5 and 8 in Table 1) are promoted during the catalytic reforming of syngas derived from thermochemical processes (Vita et al., 2018). In addition, Rh-Pt/CeO_2-SiO_2 is an effective catalyst for the conversion of CH_4 at high temperatures, owing to the presence of Rh and the high oxygen storage capacity of the CeO_2-SiO_2 support (105 μmol O_2 g_{cat}^{-1}) (Cifuentes et al., 2019). Thus, increasing the H_2/CH_4 ratio could have a positive effect on the H_2/CO mole ratio after catalytic reforming (Table 2), thereby improving both the LHV and dry gas yields (Table 2). However, in the integrated system, the H_2/CO ratio decreases by approximately 22% when going from 700 °C to 800 °C. This decrease could be associated with the thermodynamic equilibrium of WGS (Ge et al., 2016).

The CO_2/CO ratio increased compared to that in the steam gasification tests but tended to decrease with temperature (Table 2). Noble metals such as Rh and Pt promote C–C and C–H bond cleavage, leading to both H_2 and CO_2 formation (Liu et al., 2019b), which would explain the increase in CO_2/CO and H_2/CO ratios after catalytic treatment. However, the distribution of the main carbon species (CO and CO_2) during the catalytic reforming processes depends on the WGS thermodynamic equilibrium (López et al., 2013). At high temperatures (>600 °C), the reverse WGS reaction (Eq. 5 in Table 1) converts both CO_2 and H_2 formed from the reforming reaction into CO. The occurrence of reverse WGS could favor a rapid reduction in the CO_2/CO ratio with temperature. Considering the results on the H_2/CH_4 ratio, we speculate that despite the occurrence of reverse WGS at high temperatures, the conversion of CH_4 promoted by the Rh-Pt/CeO_2-SiO_2 catalystcompensates for H_2 consumption in the reverse WGS, thereby favoring the production of an H_2-rich gas with an H_2/CO ratio greater than 2.

The results suggest that Rh-Pt/CeO_2-SiO_2 is an effective catalyst for the reforming of syngas derived from steam gasification of sugarcane residual biomass. Thus, the increase in the H_2/CO, CO_2/CO, and H_2/CH_4 ratios obtained from the integrated system were ascribed to the catalyst activity during the cracking, steam reforming, and WGS reactions. Therefore, the following section discusses some characteristics of the Rh-Pt/CeO_2-SiO_2 catalyst that could influence the results presented above.

3.3. Catalyst characterization

3.3.1. Catalyst properties during syngas steam reforming

Rh-Pt/CeO_2-SiO_2 catalysts have been previously characterized in steam reforming processes (Cifuentes et al., 2016; Quiroga et al., 2020; Sanchez et al., 2016). Moreover, we present complementary characterization tests on fresh and spent samples of the Rh-Pt/CeO_2-SiO_2 catalyst to identify possible changes arising from the downstream syngas treatment. HR-TEM micrographs (Figure S1 in Supplementary Material) show that the active particles (Rh and Pt) are well dispersed on the CeO_2-SiO_2 support, forming small particles without significant changes after catalytic reforming, with an average surface-area-weighted diameter of 3.7 ± 0.8 nm. Despite the elevated temperatures involved in this study, Rh and Pt active metals did not show signs of sintering, which is an advantage over Ni-based catalysts that are susceptible to sintering in reforming processes (Sehested et al., 2001). In addition, XRD patterns (Figure S2 in Supplementary Material) and calculations of the average crystal size of CeO_2 (Table S2 in Supplementary Material) show that the support structure is not compromised after the catalytic test. Similarly, the XPS results (Figure S3 and Table S2 in Supplementary Material) show minor differences in the surface element composition and oxygen vacancies (measured in terms of Ce^{+3}/Ce^{+4} ratio) among the Rh-Pt/CeO_2-SiO_2 samples. Therefore, the Rh-Pt/CeO_2-SiO_2 catalyst stands out as a resistant material, making it a promising option for the catalytic

reforming of syngas obtained after gasification.

3.3.2. *in-situ* DRIFTS

in-situ DRIFTS tests were performed to assess the interaction between the catalyst and the main carbon species present in the syngas (CH_4, CO_2, and CO). Fig. 2a shows the DRIFTS spectra for the interaction between CH_4 and the catalyst surface. The peak at 3010 cm^{-1} is associated with the adsorption of CH_x species, and the band at 2060 cm^{-1} is related to CO adsorbed on the active metals (Rh and Pt) (Marinho et al., 2021). In the absence of an oxidizing agent in the reacting gas (a 5% CH_4/Ar mixture was used), carbonyls can be formed because of the availability of surface oxygen supplied by the catalyst support (Cobo et al., 2013). Similarly, the formation of carbonate and formate species (1200–1800 cm^{-1} in Fig. 2a), which are intermediates in CH_x and CO conversion (Cifuentes et al., 2021), is favored by the oxygen vacancies of CeO_2 (Cifuentes et al., 2020). In addition, the adsorption of CH_x, and therefore the formation of carbonyls appears to be independent of temperature, indicating that Rh-Pt/CeO_2-SiO_2 favors the conversion of CH_4 over a wide temperature range, which is in line with the increase in the H_2/CH_4 ratio observed after the catalytic treatment (Table 2).

Fig. 2b shows that O-C-O carbonates (peaks at 2345 cm^{-1} (Cifuentes et al., 2020)) appear as the main species during CO_2 adsorption. However, an increase in temperature reduces the intensity of O-C-O carbonates, showing that CO_2 has less interaction with Rh-Pt/CeO_2-SiO_2 at high temperatures and could be easily desorbed. In addition, Fig. 2c shows that initially, CO is adsorbed onto the active metals, but progressive formation of O-C-O groups is promoted by temperature, indicating that Rh-Pt/CeO_2-SiO_2 is most effective in oxidizing carbon intermediates at high temperatures. Oxygen mobility in CeO_2 is favored by temperature and the presence of a second metal oxide such as SiO_2, thereby promoting the formation of CO_2 (Cifuentes et al., 2019) that could be easily desorbed. This feature of Rh-Pt/CeO_2-SiO_2 could account for the increase in the CO_2/CO ratio (Table 2).

Fig. 2d shows the DRIFTS spectra for the interaction of a simulated syngas (CH_4, CO, CO_2, Ar, and water) with the catalyst surface. The intensity and variety of carbonate and formate species (C-O* zone) increased significantly when the gas mixture interacted with the catalyst compared to the independent interactions between CH_4, CO_2, and CO.

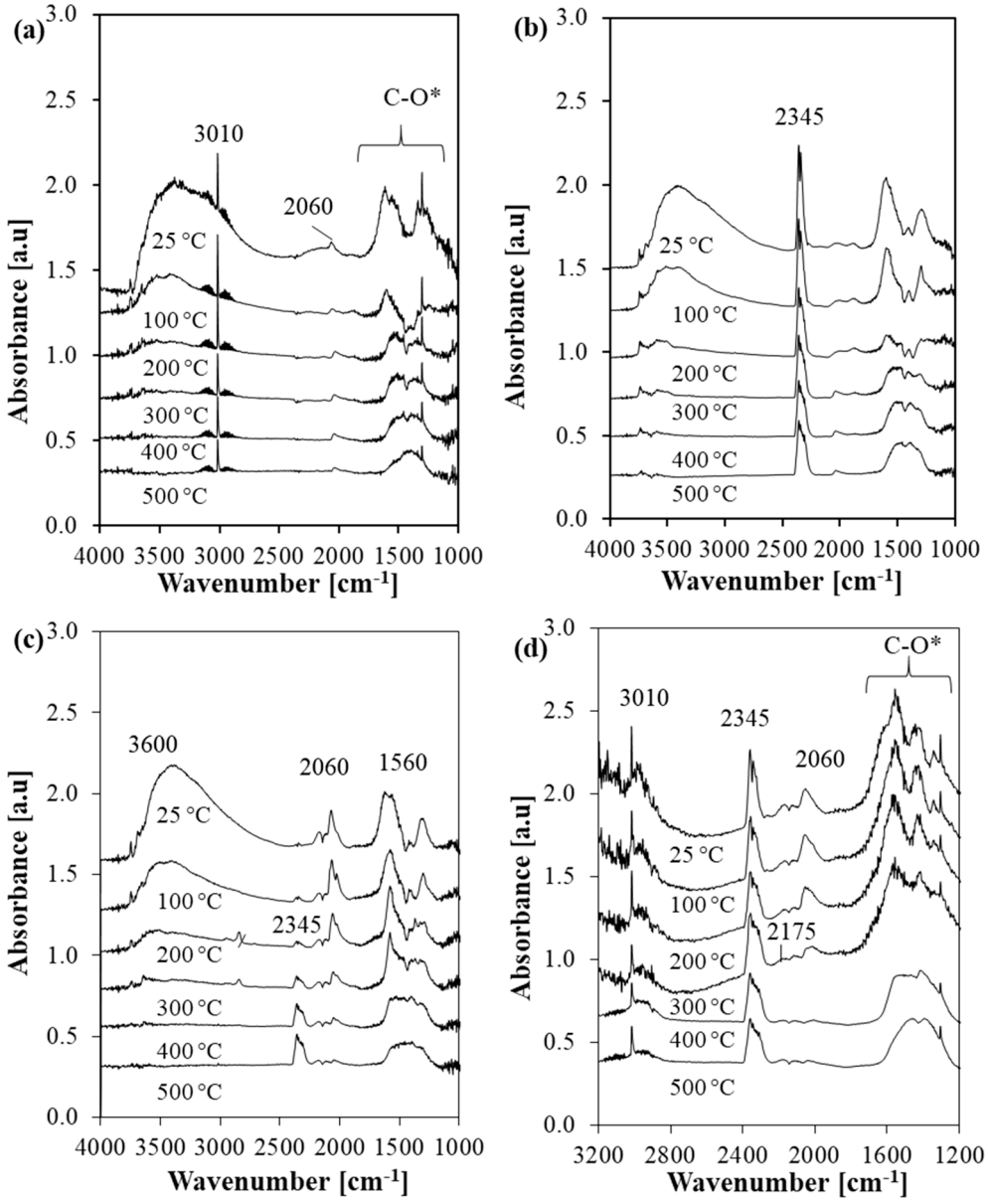

Fig. 2. *in-situ* DRIFT for the adsorption of (a) CH_4, (b) CO_2, (c) CO and (d) a simulate syngas (mixture of 5% CH_4, 5% CO, 5% CO_2 and Ar saturated with water) over Rh-Pt/CeO_2-SiO_2 catalyst.

Note that the hydroxyl groups (band centered at 3600 cm^{-1}) that were formed during the catalyst reduction pretreatment, are desorbed rapidly with temperature (Fig. 2a, b, and c). These hydroxyls are important intermediates in the oxidation of CO (Cifuentes et al., 2021). Subsequently, a deficiency in hydroxyl groups could negatively impact the activity of the catalyst. In Fig. 2d, the hydroxyl band was not included because of the significant increase observed, which made the analysis of other zones more difficult. The formation of hydroxyl groups is associated with the presence of water in the simulated syngas, which could compensate for the desorption of these species (i.e. hydroxyls) with temperature. Consequently, the change in carbon intermediates in the simulated syngas could be associated with an increase in the number of surface hydroxyls formed from water. In addition, the adsorption of water over SiO_2-based materials favors water splitting, thereby producing additional H_2 (Cifuentes et al., 2019).

Therefore, the presence of stable active metals, such as Rh and Pt, to reform hydrocarbons together with a CeO_2-SiO_2 support, which supplies surface oxygen and favors the formation of hydroxyl groups, contributes to the production of a H_2-rich syngas after catalytic reforming. Nevertheless, the sustainability of the gasification technology depends not only on the production of H_2-rich syngas, but also on its effectiveness in mitigating pollutant emissions. In the upcoming sections, several pollutants involved in the thermic processes involved are screened during gasification and gasification/reforming tests.

3.4. Formation of pollutants during gasification and gasification/reforming of residual biomass

3.4.1. Light HC and BTEX formation

Light HCs and BTEX are important by-products formed during steam gasification. The formation of excessive amounts of these compounds could be evidence of low selectivity during gasification. Table 2 shows that light HCs and BTEX constitute up to 14% of the syngas produced by steam gasification at 700 °C. Table 3 details the yields for the most common light HCs formed during thermochemical processes, including dangerous compounds such as BTEX. No clear trends in the formation of each light HC or BTEX were identified, because of the complex network of chemical reactions occurring during gasification. However, the total concentration of light HCs and BTEX increased by a factor of three (approximately) between 600 and 800 °C (Table 3), indicating that at high temperatures, steam gasification would be most likely to favor the formation of dangerous compounds.

After catalytic reforming, the total amount of light HCs and BTEX (Table 3) decreased by up to 62% at 800 °C. The favoring of cracking and reforming reactions by the catalyst could contribute to the conversion of light HCs (Farooq et al., 2021; Vita et al., 2018), thereby increasing H_2 yield (Table 2), and reducing pollutants. Also, the decrease of the light HCs at 800 °C could be related to the longer residence time due to the catalytic bed that favors decomposition of some HCs and tars (Nguyen et al., 2018). These results coincide with a study by Hernandez et al. in which they evaluated the effect of residence time on H_2 production from biomass and reported that a residence time increase of 1.4 times leads to a H_2 increase of 2.5 times when approaching equilibrium (Hernández et al., 2010). At higher temperatures, where steam gasification favored light HC and BTEX formation the most (Table 2), catalytic reforming of syngas over Rh-Pt/CeO_2-SiO_2 catalyst is effective in removing mainly propylene, butanes, butenes, propyne, butynes, n-hexane, benzene, and xylenes (Table 3). This coincides with the results of a study by Nguyen et al., who reported the total elimination of acetylene (C_2H_2) and propylene (C_3H_6) and approximately 46% of ethylene (C_2H_4) conversion in syngas after a catalytic treatment at 800 °C with ilmenite as the catalyst (Nguyen et al., 2018). Similarly, Savuto et al. reported the conversion of benzene (>60%) over Ni/Mayenite at 800 °C during the steam catalytic reforming of syngas from biomass gasification (Savuto et al., 2017). However, the structure and stability of contaminants influence the effectiveness of their removal during downstream treatments. Table 3 shows that some light HCs and toluene increased in concentration after catalytic reforming, possibly due to the decomposition of naphthalene and acenaphthene (Nguyen et al., 2018). Thus, some hazardous contaminants may require additional treatment, to effectively remove them.

Table 3
Light HCs and BTEX compounds formed during steam gasification and after catalytic reforming of syngas. Mean values ± standard deviation of the measurements are shown.

Aspect	Outlet stream					
	Gasification			Catalytic reforming		
	G-600	G-700	G-800	GR-600	GR-700	GR-800
Light HCs [mg compound $kg_{biomass}^{-1}$ (ppm)]						
Ethane	3,730 ± 30	5,890 ± 40	6,700 ± 500	3,912 ± 10	5,630 ± 70	4,500 ± 30
Ethylene	181.6 ± 1.3	688 ± 4	1,090 ± 180	161.6 ± 0.4	530 ± 7	627 ± 4
Propane	1,093 ± 8	1,299 ± 8	680 ± 110	1,289 ± 4	1,106 ± 15	378 ± 2
Propylene	96.3 ± 0.7	318 ± 2	240 ± 40	93.9 ± 0.2	231 ± 3	101.3 ± 0.7
Isobutane	nd	nd	13,300 ± 900	nd	47.8 ± 0.2	nd
Acetylene	91.3 ± 0.6	4,328 ± 17	nd	101.9 ± 1.4	2,400 ± 60	5,610 ± 50
n-butane	412 ± 2	968 ± 9	1,700 ± 300	186.4 ± 0.6	661 ± 9	502 ± 7
1-butene	nd	nd	nd	nd	nd	nd
trans-2-butene	7,940 ± 50	19,880 ± 120	1,600 ± 200	7,650 ± 30	8,190 ± 100	325 ± 5
Isobutene	491 ± 3	936 ± 6	500 ± 80	516 ± 2	705 ± 7	209 ± 3
cis-2-butene	219.3 ± 0.8	495 ± 3	180 ± 30	252 ± 2	385 ± 4	64.5 ± 0.8
Isopentane	nd	21.16 ± 0.12	nd	nd	18.5 ± 0.5	nd
n-pentane	27.1 ± 1.0	14,820 ± 120	83 ± 9	34.3 ± 0.3	185 ± 2	nd
Propyne	480 ± 4	nd	28,700 ± 400	645 ± 2	18,900 ± 300	55.80 ± 0.05
1,3-butadiene	7,030 ± 50	nd	nd	7,270 ± 40	nd	11,800 ± 100
1-pentene	15.8 ± 0.13	6.70 ± 0.03	0.147 ± 0.014	16.77 ± 0.09	2.27 ± 0.03	nd
2-butyne	305.1 ± 0.6	2,270 ± 30	3,700 ± 600	564 ± 4	1,000 ± 7	912 ± 7
1-butyne	96.5 ± 0.4	222.5 ± 1.4	90 ± 19	16.37 ± 0.10	83 ± 3	22 ± 2
n-hexane	904 ± 6	3,790 ± 50	3,800 ± 600	900 ± 400	2,790 ± 30	1,828 ± 15
1-hexene	9.82 ± 0.014	2.72 ± 0.04	2.3 ± 0.3	12.77 ± 0.12	0.64 ± 0.03	0.64 ± 0.02
cis-2-hexene	31.7 ± 0.5	34.8 ± 0.9	23 ± 4	39.4 ± 0.7	12.9 ± 0.9	5.747 ± 0.003
n-heptane	11 ± 2	120 ± 10	29 ± 6	22.76 ± 0.04	78 ± 5	nd
1-heptene	nd	nd	nd	nd	nd	nd
Isooctane	3.1 ± 1.0	8.5 ± 0.5	4.85 ± 0.02	5 ± 4	5 ± 3	nd
Benzene	64.9 ± 0.4	240 ± 100	31 ± 4	58 ± 4	160 ± 120	10.3 ± 0.3
Toluene	nd	4,830 ± 50	980 ± 80	250 ± 150	2,020 ± 18	1,161 ± 14
Xylene (p-, m-,o-)	1,600 ± 200	316 ± 16	13,400 ± 900	nd	6,480 ± 180	109 ± 5
Total Light HCs and BTEX	24900 ± 400	61500 ± 400	76700 ± 900	23700 ± 700	51600 ± 700	28200 ± 200

nd: not detected or lower than the detection limit (1 mg $kg_{biomass}^{-1}$).

3.4.2. PAHs

Tars are also undesirable compounds formed during gasification, especially PAHs, owing to their negative impact on the environment. Similar to light HCs, PAHs tend to increase with temperature, reaching

up to 11 g Nm^{-3} of tar yield and 3930 mg $kg^{-1}_{biomass}$ of total PAHs (see the yields of the 16 priority PAHs in Table 4). Zhang et al. evaluated PAH production during steam gasification of different biomass materials and reported that above 700 °C, PAH formation exponentially increases due to the change from light tar compounds and BTEX into PAHS with an increase in temperature from 700 to 800 °C (Zhang and Pang, 2019). In addition, Aljbour et al. (Aljbour and Kawamoto, 2013) evaluated the gasification of cedar biomass gasification, mentioning that between 700 and 900 °C, the concentrations of naphthalene, fluorine, phenanthrene, and anthracene increased because temperature favored the formation of radicals, which are intermediates for light PAH production. Therefore, despite favoring biomass conversion and increasing H_2 concentration in the syngas (Table 2), temperature also promoted PAHs emissions during steam gasification.

After catalytic reforming, most of the tars decreased by approximately 60% compared to steam gasification (Table 4). Tomishige et al. (Tomishige et al., 2003) found that the order of catalytic activity of metals supported on CeO_2–SiO_2 for the reforming of tar derived from cedar biomass was Rh > Pt > Pd > Ni, achieving 77% tar conversion at 700 °C with Rh/CeO_2-SiO_2. In addition, Kobayashi et al. studied the influence of silica (SiO_2) as a catalyst to remove tars from syngas, reporting that heavy PAHs are easily decomposed over SiO_2 owing to its high surface area (100–300 m^2 g^{-1}) (Kobayashi et al., 2019). Therefore, the Rh-Pt/CeO_2-SiO_2 catalyst could favor tar conversion during steam reforming of syngas owing to the presence of highly active metals (Rh and Pt) and the high surface area of the support (the catalyst used in this work has a surface area of 104 m^2 g^{-1}_{cat}).

Fig. 3a shows the efficiency of PAH removal during catalytic treatment. Most PAHs, including naphthalene (the main PAH produced during gasification, according to Table 4) were reduced after steam reforming over the Rh-Pt/CeO_2-SiO_2 catalyst, mainly at 800 °C. However, for the removal of other compounds such as acenaphthylene, acenaphthene, fluoranthene, and pyrene, temperatures below 800 °C would be more suitable. Liu et al. suggested that the reforming of PAHs depends on their chemical structure: smaller hydrocarbon aromatics are more difficult to remove by steam reforming compared to aromatics with larger rings or O-containing groups (Liu et al., 2021). In addition, as discussed in the DRIFTS tests, the water present in the syngas could be adsorbed into the catalyst surface and form active radicals (e.g., H*, OH^-, and O*), which are needed to reform small tar molecules (Liu et al., 2021). However, an increase in gasification temperature is expected to favor the conversion of water in endothermic steam reforming reactions (Cifuentes et al., 2020), which leads to a reduction in the availability of water for catalytic reforming. Thus, the amount of water in the syngas may decrease when gasification is carried out at high temperatures, which can reduce the effectiveness in removing some PAHs during catalytic reforming. Despite the differences observed with the process temperature, catalytic reforming after gasification is a promising strategy to reduce both light HCs and tars in the syngas obtained from biomass.

Table 4
PAH yields for single gasification and after catalytic reforming of syngas.

Compound	Tar compound yields mg $kg^{-1}_{biomass}$					
	G-600	G-700	G-800	GR-600	GR-700	GR-800
Naphthalene	193	804	2070	129	642	1230
Acenaphthylene	20	200	575	12	124	450
Acenaphthene	13	54	49	15	28	39
Fluorene	29	79	185	24	61	201
Phenanthrene	40	144	376	22	137	275
Anthracene	9	36	130	5	26	82
Fluoranthene	7	19	76	4	15	50
Pyrene	12	30	183	6	29	161
Benzo(a)anthracene	6	16	85	3	10	38
Chrysene	18	44	105	10	38	66
Benzo(b)fluoranthene	5	3	17	nd	2	7
Benzo(k)fluoranthene	nd	2	23	2	2	11
Benzo(a)pyrene	4	7	39	1	4	16
Indene(1,2,3-cd) pyrene	nd	nd	10	nd	nd	4
Dibenzo(a,h) anthracene	nd	nd	nd	nd	nd	nd
Benzo(g,h,i)perylene	nd	nd	9	nd	2	4
Total PAHs [mg $kg^{-1}_{biomass}$]	354	1440	3930	234	1120	2640
Tar yield [g Nm^{-3}]	2.4	8.4	10.9	0.9	2.9	3.6

nd: not detected or lower than the detection limit (1 mg $kg^{-1}_{biomass}$).

3.4.3. PCDD/Fs

The previous sections showed that high temperatures (700–800 °C) are necessary to obtain a H_2-rich syngas (*Vide ante*); therefore, dioxin analysis was performed only for gasification with and without catalyst at 700 and 800 °C. Dioxins and furans can be formed during thermochemical processes (Conesa et al., 2020) from pyrosynthesis reactions, promoted by the presence of chlorinated aromatic hydrocarbons under oxidation conditions and high temperatures (400–800 °C) (Rathna et al., 2018). Conesa et al. reviewed pollutant emissions during pyrolysis and incineration/gasification of industrial waste, and reported that under poor oxygenation conditions, incomplete oxidation of carbon species is favored, leading to the formation of an excessive amount of PCDD/F (Conesa et al., 2020). However, the authors also mention that biomass resources such as cotton waste produced significantly less pollutants compared to electronic waste and polyvinyl chloride (PVC)-based materials. This coincides with our results (Table S3 in Supplementary Material), where a PCDD/F concentration lower than 32.5 ng WHO-TEQ Nm^{-3} was recorded during gasification of sugarcane residual biomass at 800 °C. Although, the presence of PCDD/F, even in low concentrations in the outlet streams of could cause health and environmental risks. Fig. 3b shows the efficiency of the Rh-Pt/CeO_2-SiO_2 catalyst in the removal of PCDD/Fs from the syngas derived from gasification. At 800 °C, the PCDD/F concentration is reduced due to decomposition of most of the congeners, while at 700 °C, the emissions of 2,3,7,8-TCDF, 1,2,3,7,8-PeCDF, 2,3,4,7,8-PeCDF, and 1,2,3,7,8-PeCDD increased during catalytic reforming. Thus, at 700 °C, the Rh-Pt/CeO_2-SiO_2 catalyst favored the decomposition of higher dioxins, but it also favored the formation of more toxic compounds. The above could be related to the correlation of dioxin formation with temperature, since it has been shown that with an increase in temperature the decomposition of PCDD/Fs is higher (Kawamoto et al., 2009; Maric et al., 2020). However, at 800 °C, catalytic reforming promotes decomposition of all of PCDD/Fs, reducing the total toxicity of the stream to 1.8 ng WHO-TEQ Nm^{-3} (Table S3 in Supplementary Material). Steam gasification is a process with poor oxygen presence (as the only oxygen present comes from the biomass), which makes it difficult to compare with the standard 11% O_2 used to determine the legal limits in combustion processes (Conesa et al., 2020).

Table 5 compares the removal efficiencies of several pollutants using different catalytic reforming systems. Most studies have focused on evaluating the elimination of tars/PAHs, using mainly tar model streams (a synthetic mix of some PAHs), which report conversions higher than 87% (Qian and Kumar, 2017). However, PAHs derived from an actual gasification stream could be more difficult to reform depending on the biomass source and the presence of additional contaminants, which may decrease the PAH-removal efficiency (to as little as 20% in some cases) (Nguyen et al., 2018).

However, information about the formation and elimination of PCDD/Fs during steam reforming is limited. Bangala et al. (1997) used o-dichlorobenzene (a compound with a chemical structure similar to 2,3,7,8-TCDD) as a molecular model to assess the effectiveness of a UCI-GB 98 commercial catalyst in the elimination of dioxins by steam reforming, and reported the total conversion of dichlorobenzene at 850 °C. There have been no other reports on the elimination or formation of PCDD/Fs. Although we found that under certain conditions, some

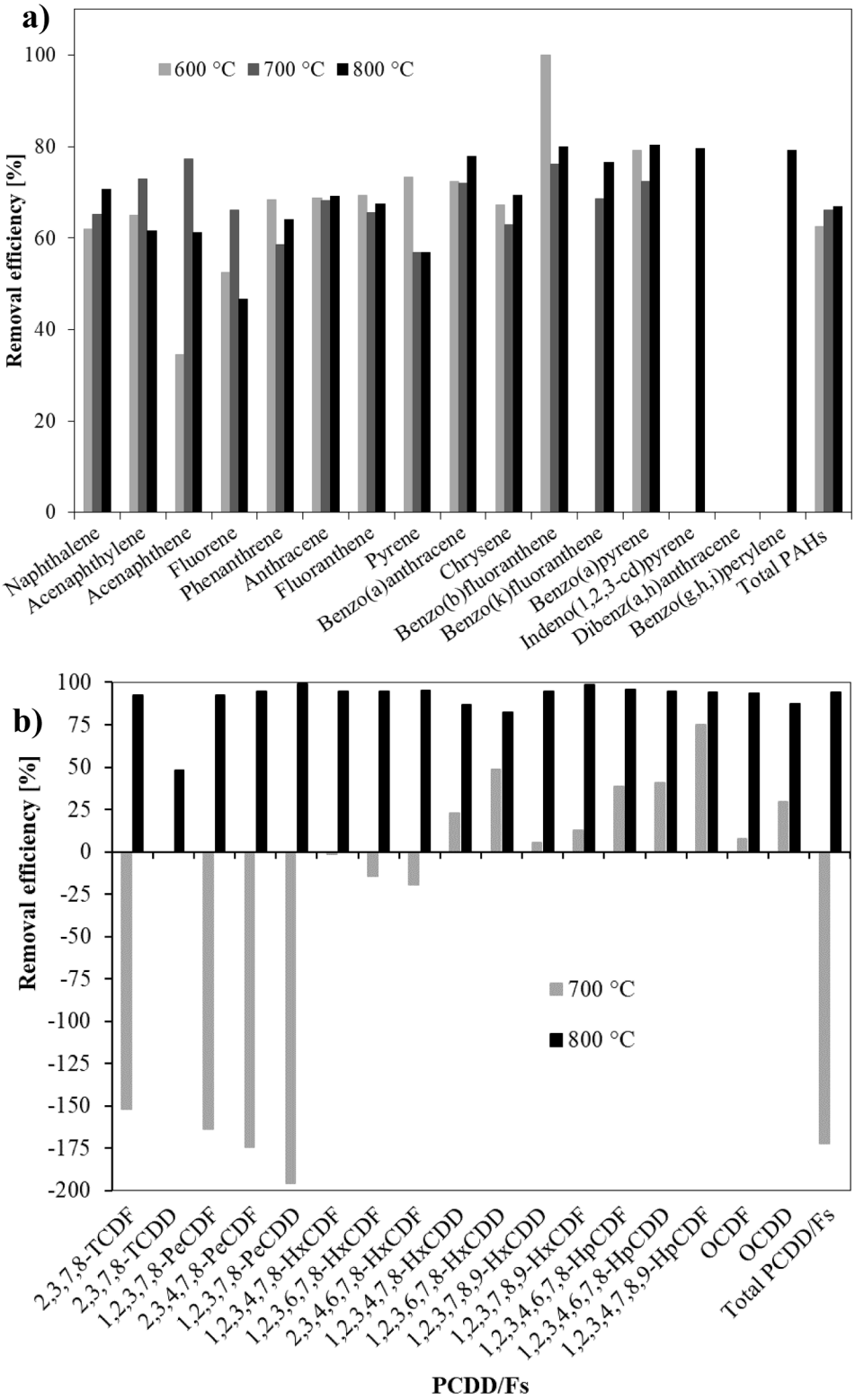

Fig. 3. Removal efficiency of (a) PAH ad (b) PCDD/F, during catalytic reforming of syngas derived from gasification.

dioxins could be formed during steam reforming, 94% of PCDD/Fs in the syngas were removed at 800 °C after catalytic reforming over the Rh-Pt/CeO_2-SiO_2 catalyst.

Therefore, catalytic reforming of syngas obtained from biomass gasification presents promising features for the improvement of the H_2 concentration in syngas, leading to an increase in the H_2/CO molar ratio and a decrease in most of the pollutants formed. Thus, the catalytic treatment after the gasifier could be an essential step to expand the possibilities of using the syngas obtained from lignocellulosic biomass, especially for its use in energy applications, and to reduce the adverse environmental impact associated with the emission of pollutants.

Table 5
Comparison of pollutant removal efficiency by catalytic reforming.

Inlet stream	T (°C)	Catalyst	Removal efficiency (%)			Reference
			Light HCs/ BTEX	Tars/ PAHs	PCDD/ Fs	
Tar model that includes benzene, toluene and naphthalene	850	Activated biochar	NR	90	NR	(Buentello-Montoya et al., 2020)
Tar model that includes toluene and naphthalene	800	Ni/Activated char	NR	~87	NR	(Qian and Kumar, 2017)
Tar model based on naphthalene	700	Activated bauxite residue	NR	~98	NR	(Cheng et al., 2020)
Tars obtained from woody biomass gasification	800	Ilmenite	NR	20	NR	(Nguyen et al., 2018)
Tars obtained from cedar wood gasification	550	$Ni/CeO_2–SiO_2$	NR	89	NR	(Tomishige et al., 2003)
Tars obtained from cedar wood gasification	550	$Rh/CeO_2–SiO_2$	NR	100	NR	(Tomishige et al., 2003)
Tars obtained from woody waste gasification	850	Porous silica	NR	~38	NR	(Kobayashi et al., 2019)
Syngas obtained from gasification of pine pellets	800	$Ni/MgAl_2O_4$	~25	~80	NR	(Hernandez et al., 2020)
Syngas obtained from gasification of sewage sludge - coal blends	900	$Ni/CaO/La\text{-}Al_2O_3$	NR	100	NR	(García et al., 2013)
Gas model that includes naphthalene and dichlorobenzene	850	UCI-GB 98 commercial	NR	100	100*	(Bangala et al., 1997)
Syngas obtained from gasification of sugarcane residual biomass	800	$Rh\text{-}Pt/CeO_2\text{-}SiO_2$	60	60	94	This work

NR: Not reported.
*Dichlorobenzene was used as a model compound to evaluate dioxin reforming.

4. Conclusions

Catalytic reforming over a $Rh\text{-}Pt/CeO_2\text{-}SiO_2$ catalyst was evaluated as a downstream treatment process for syngas obtained from gasification of biomass. Syngas obtained from steam gasification has a low H_2/CO ($\leq$0.8) ratio. However, the inclusion of a catalytic reforming step after gasification promoted the conversion of hydrocarbons present in the syngas, thereby increasing the energy density of the outlet gas stream (LHV yield increased up to 2.3 times) and enabling the production of syngas with a H_2 concentration of up to 37% and H_2/CO ratios $\geq$ 2. In addition, notwithstanding the high temperatures at which catalytic reforming was carried out (>600 °C), characterization tests revealed that the $Rh\text{-}Pt/CeO_2\text{-}SiO_2$ catalyst was neither susceptible to the sintering of its active metals, nor to significant changes in the crystal size of CeO_2, or variations in the surface element composition, thereby making it a stable material for reforming processes. Likewise, *in-situ* DRIFTS tests showed that the presence of steam and surface oxygen over the $Rh\text{-}Pt/CeO_2\text{-}SiO_2$ catalyst promotes the formation and oxidation of carbon intermediates, favoring the conversion of CH_4 and other hydrocarbons, including pollutants. These characteristics of $Rh\text{-}Pt/CeO_2\text{-}SiO_2$ make it a promising catalyst for the reforming of syngas from thermochemical processes.

On the other hand, the syngas obtained after steam gasification contained important amounts of pollutants, reaching up to 14.5 mol% concentration of light HCs and BTEX, 10.9 g Nm^{-3} of tars, and 25 pg WHO-TEQ $g^{-1}_{biomass}$ of PCDD/Fs. Likewise, catalytic reforming promotes the elimination of most pollutants, removing up to 62% of light HCs and BTEX, 60% of PAHs, and 94% of PCDD/Fs. The improvement in syngas H_2-yield and overall quality during the integrated process (gasification followed by catalytic reforming) contributes to expanding the possibilities of using syngas obtained from residual biomass in energy applications.

Declaration of Competing Interest

The authors declare that they have no known competing financial interests or personal relationships that could have appeared to influence the work reported in this paper.

Acknowledgments

The authors are grateful to Universidad de La Sabana (Project code ING-203-2018), the Spanish Ministry of Science and Innovation (State Investigation Agency, project code PID2019-108632RB-I00), and The International Relations Department of the University of Alicante (program named “University Development Cooperation 2019”) for their financial support toward this work. The GC-MS/QQQ used in the analysis was supported by Project IDIFEDER/2018/004 by the Generalitat Valenciana (Spain).

Appendix A. Supplementary material

Supplementary data to this article can be found online at https://doi.org/10.1016/j.wasman.2022.05.012.

References

Aljbour, S.H., Kawamoto, K., 2013. Bench-scale gasification of cedar wood - Part II: Effect of Operational conditions on contaminant release. Chemosphere 90 (4), 1501–1507. https://doi.org/10.1016/j.chemosphere.2012.08.030.

AlQattan, N., Acheampong, M., Jaward, F.M., Ertem, F.C., Vijayakumar, N., Bello, T., 2018. Reviewing the potential of Waste-to-Energy (WTE) technologies for Sustainable Development Goal (SDG) numbers seven and eleven. Renew. Energy Focus 27, 97–110. https://doi.org/10.1016/j.ref.2018.09.005.

Anniwaer, A., Chaihad, N., Zhang, M., Wang, C., Yu, T., Kasai, Y., Abudula, A., Guan, G., 2021. Hydrogen-rich gas production from steam co-gasification of banana peel with agricultural residues and woody biomass. Waste Manag. 125, 204–214. https://doi.org/10.1016/J.WASMAN.2021.02.042.

Asadullah, M., Ito, S.-I., Kunimori, K., Yamada, M., Tomishige, K., 2002. Biomass gasification to hydrogen and syngas at low temperature: Novel catalytic system using fluidized-bed reactor. J. Catal. 208 (2), 255–259. https://doi.org/10.1006/jcat.2002.3575.

Bangala, D.N., Abatzoglou, N., Martin, J.P., Chornet, E., 1997. Catalytic Gas Conditioning: Application to Biomass and Waste Gasification. Ind. Eng. Chem. Res. 36, 4184–4192. https://doi.org/10.1021/ie960785a.

Buentello-Montoya, D., Zhang, X., Li, J., Ranade, V., Marques, S., Geron, M., 2020. Performance of biochar as a catalyst for tar steam reforming: Effect of the porous structure. Appl. Energy 259, 114176. https://doi.org/10.1016/j.apenergy.2019.114176.

Cavusoglu, G., Miao, D., Lichtenberg, H., Carvalho, H.W.P., Xu, H., Goldbach, A., Grunwaldt, J.-D., 2015. Structure and activity of flame made ceria supported Rh and Pt water gas shift catalysts. Appl. Catal. A Gen. 504, 381–390. https://doi.org/10.1016/J.APCATA.2015.01.047.

Cheng, L., Wu, Z., Zhang, Z., Guo, C., Ellis, N., Bi, X., Paul Watkinson, A., Grace, J.R., 2020. Tar elimination from biomass gasification syngas with bauxite residue derived catalysts and gasification char. Appl. Energy 258, 114088. https://doi.org/10.1016/j.apenergy.2019.114088.

Cifuentes, B., Bustamante, F., Araiza, D.G., Diaz, G., Cobo, M., 2020. Hydrogen purification of actual syngas streams for energy applications: Au-Cu supported over nano-shaped CeO_2 as stable catalysts for the carbon monoxide removal. Appl. Catal. A Gen. 598, 117568–1157581. https://doi.org/10.1016/j.apcata.2020.117568.

Cifuentes, B., Bustamante, F., Cobo, M., 2019. Single and dual metal oxides as promising supports for carbon monoxide removal from an actual syngas: The crucial role of support on the selectivity of the au–cu system. Catalysts 9, 852. https://doi.org/10.3390/catal9100852.

Cifuentes, B., Gómez, J., Sánchez, N., Proaño, L., Bustamante, F., Cobo, M., 2021. Bioethanol steam reforming over monoliths washcoated with $RhPt/CeO_2–SiO_2$: The

use of residual biomass to stably produce syngas. Int. J. Hydrogen Energy 46 (5), 4007–4018. https://doi.org/10.1016/j.ijhydene.2020.10.271.
Cifuentes, B., Hernández, M., Monsalve, S., Cobo, M., 2016. Hydrogen production by steam reforming of ethanol on a RhPt/CeO_2/SiO_2 catalyst: Synergistic effect of the Si: Ce ratio on the catalyst performance. Appl. Catal. A Gen. 523, 283–293 https://doi.org/https://doi.org/10.1016/j.apcata.2016.06.014.
Cobo, M., Pieruccini, D., Abello, R., Ariza, L., Córdoba, L.F., Conesa, J. a., 2013. Steam reforming of ethanol over bimetallic RhPt/La2O3: Long-term stability under favorable reaction conditions. Int. J. Hydrogen Energy 38, 5580–5593. https://doi.org/10.1016/j.ijhydene.2013.02.044.
Conesa, J.A., Ortuño, N., Palmer, D., 2020. Estimation of Industrial Emissions during Pyrolysis and Combustion of Different Wastes Using Laboratory Data. Sci. Rep. 10, 1–11. https://doi.org/10.1038/s41598-020-63807-w.
Edo, M., Ortuño, N., Persson, P.E., Conesa, J.A., Jansson, S., 2018. Emissions of toxic pollutants from co-combustion of demolition and construction wood and household waste fuel blends. Chemosphere 203, 506–513. https://doi.org/10.1016/j.chemosphere.2018.03.203.
Farooq, A., Moogi, S., Jang, S.H., Kannapu, H.P.R., Valizadeh, S., Ahmed, A., Lam, S.S., Park, Y.K., 2021. Linear low-density polyethylene gasification over highly active Ni/CeO_2-ZrO_2 catalyst for enhanced hydrogen generation. J. Ind. Eng. Chem. 94, 336–342. https://doi.org/10.1016/j.jiec.2020.11.005.
Fremaux, S., Beheshti, S.M., Ghassemi, H., Shahsavan-Markadeh, R., 2015. An experimental study on hydrogen-rich gas production via steam gasification of biomass in a research-scale fluidized bed. Energy Convers. Manag. 91, 427–432. https://doi.org/10.1016/j.enconman.2014.12.048.
Gandon-Ros, G., Nuñez, S.S., Ortuño, N., Aracil, I., Gómez-Rico, M.F., Conesa, J.A., 2021. A win–win combination to inhibit persistent organic pollutant formation via the co-incineration of polyvinyl chloride e-waste and sewage sludge. Polymers (Basel). 13, 1–17. https://doi.org/10.3390/polym13050835.
García, G., Monzón, A., Bimbela, F., Sánchez, J.L., Ábrego, J., 2013. Desulfurization and catalytic gas cleaning in fluidized-bed co-gasification of sewage sludge-coal blends. Energy Fuels 27 (5), 2846–2856. https://doi.org/10.1021/ef400259g.
Ge, H., Guo, W., Shen, L., Song, T., Xiao, J., 2016. Experimental investigation on biomass gasification using chemical looping in a batch reactor and a continuous dual reactor. Chem. Eng. J. 286, 689–700. https://doi.org/10.1016/j.cej.2015.11.008.
He, J., Yang, Z., Xiong, S., Guo, M., Yan, Y., Ran, J., Zhang, L., 2020. Experimental and thermodynamic study of banana peel non-catalytic gasification characteristics. Waste Manag. 113, 369–378. https://doi.org/10.1016/J.WASMAN.2020.06.006.
Hernandez, A., Andersson, K.J., Engvall, K., Kantarelis, E., 2020. Gas-Phase Potassium Effects and the Role of the Support on the Tar Reforming of Biomass-Derived Producer Gas over Sulfur-Equilibrated Ni/$MgAl_2O_4$. Energy and Fuels 34 (9), 11103–11111. https://doi.org/10.1021/acs.energyfuels.0c02069.
Hernández, J.J., Aranda-Almansa, G., Bula, A., 2010. Gasification of biomass wastes in an entrained flow gasifier: Effect of the particle size and the residence time. Fuel Process. Technol. 91 (6), 681–692. https://doi.org/10.1016/j.fuproc.2010.01.018.
Hernández, J.J., Ballesteros, R., Aranda, G., 2013. Characterisation of tars from biomass gasification: Effect of the operating conditions. Energy 50, 333–342. https://doi.org/10.1016/j.energy.2012.12.005.
Hiblot, H., Ziegler-Devin, I., Fournet, R., Glaude, P.A., 2016. Steam reforming of methane in a synthesis gas from biomass gasification. Int. J. Hydrogen Energy 41 (41), 18329–18338. https://doi.org/10.1016/j.ijhydene.2016.07.226.
Hu, J., Li, D., Lee, D.-J., Zhang, Q., Wang, W., Zhao, S., Zhang, Z., He, C., 2019. Integrated gasification and catalytic reforming syngas production from corn straw with mitigated greenhouse gas emission potential. Bioresour. Technol. 280, 371–377. https://doi.org/10.1016/j.biortech.2019.02.064.
Hu, M., Guo, D., Ma, C., Hu, Z., Zhang, B., Xiao, B., Luo, S., Wang, J., 2015. Hydrogen-rich gas production by the gasification of wet MSW (municipal solid waste) coupled with carbon dioxide capture. Energy 90, 857–863. https://doi.org/10.1016/J.ENERGY.2015.07.122.
Huang, Z., He, F., Zheng, A., Zhao, K., Chang, S., Zhao, Z., Li, H., 2013. Synthesis gas production from biomass gasification using steam coupling with natural hematite as oxygen carrier. Energy 53, 244–251. https://doi.org/10.1016/j.energy.2013.02.068.
Hwang, I.-H., Kobayashi, J., Kawamoto, K., 2014. Characterization of products obtained from pyrolysis and steam gasification of wood waste, RDF, and RPF. Waste Manag. 34 (2), 402–410. https://doi.org/10.1016/j.wasman.2013.10.009.
Irfan, M., Li, A., Zhang, L., Ji, G., Gao, Y., Khushk, S., 2021. Hydrogen-rich syngas from wet municipal solid waste gasification using Ni/Waste marble powder catalyst promoted by transition metals. Waste Manag. 132, 96–104. https://doi.org/10.1016/J.WASMAN.2021.07.019.
Izquierdo, U., Barrio, V.L., Bizkarra, K., Gutierrez, A.M., Arraibi, J.R., Gartzia, L., Bañuelos, J., Lopez-Arbeloa, I., Cambra, J.F., 2014. Ni and RhNi catalysts supported on Zeolites L for hydrogen and syngas production by biogas reforming processes. Chem. Eng. J. 238, 178–188. https://doi.org/10.1016/j.cej.2013.08.093.
Izquierdo, U., García-García, I., Barrio, V.L., Cambra, J.F., 2017. Hydrogen Production with a Microchannel Reactor by Tri-Reforming; Reaction System Comparison and Catalyst Development. Top. Catal. 60 (15-16), 1210–1225. https://doi.org/10.1007/s11244-017-0798-9.
Katsaros, G., Pandey, D.S., Horvat, A., Almansa, G.A., Fryda, L.E., Leahy, J.J., Tassou, S. A., 2019. Gasification of poultry litter in a lab-scale bubbling fluidised bed reactor: Impact of process parameters on gasifier performance and special focus on tar evolution. Waste Manag. 100, 336–345. https://doi.org/10.1016/j.wasman.2019.09.014.
Kawamoto, K., Wu, W., Kuramochi, H., 2009. Development of Gasification and Reforming Technology using Catalyst at Lower Temperature for Effective Energy Recovery: Hydrogen Recovery Using Waste Wood. J. Environ. Eng. 4 (2), 409–421. https://doi.org/10.1299/jee.4.409.
Kobayashi, J., Kawamoto, K., Kobayashi, N., 2019. Effect of porous silica on the removal of tar components generated from waste biomass during catalytic reforming. Fuel Process. Technol. 194, 106104–106119. https://doi.org/10.1016/j.fuproc.2019.05.027.
Lalsare, A., Wang, Y., Li, Q., Sivri, A., Vukmanovich, R.J., Dumitrescu, C.E., Hu, J., 2019. Hydrogen-Rich Syngas Production through Synergistic Methane-Activated Catalytic Biomass Gasification. ACS Sustain. Chem. Eng. 7 (19), 16060–16071. https://doi.org/10.1021/acssuschemeng.9b0266310.1021/acssuschemeng.9b02663.s001.
Lin, C., Weng, W., 2017. Effects of different operating parameters on the syngas composition in a two-stage gasi fi cation process. Renew. Energy 109, 135–143. https://doi.org/10.1016/j.renene.2017.03.019.
Liu, L., Zhang, Z., Das, S., Kawi, S., 2019a. Reforming of tar from biomass gasification in a hybrid catalysis-plasma system: A review. Appl. Catal. B Environ. 250, 250–272. https://doi.org/10.1016/j.apcatb.2019.03.039.
Liu, X., Wang, K., Zhou, Y., Zhang, X., Tang, X., Ren, P., Jiang, X., Liu, B., 2019b. In-situ fabrication of Ce-rich CeO_2 nanocatalyst for efficient CO oxidation. J. Alloys Compd. 792, 644–651. https://doi.org/10.1016/j.jallcom.2019.04.057.
Liu, Y., Paskevicius, M., Wang, H., Parkinson, G., Wei, J., Asif Akhtar, M., Li, C.Z., 2021. Insights into the mechanism of tar reforming using biochar as a catalyst. Fuel 296, 120672–120688. https://doi.org/10.1016/j.fuel.2021.120672.
López, E., Divins, N.J., Anzola, A., Schbib, S., Borio, D., Llorca, J., 2013. Ethanol steam reforming for hydrogen generation over structured catalysts. Int. J. Hydrogen Energy 38 (11), 4418–4428. https://doi.org/10.1016/j.ijhydene.2013.01.174.
Maric, J., Berdugo Vilches, T., Pissot, S., Cañete Vela, I., Gyllenhammar, M., Seemann, M., 2020. Emissions of dioxins and furans during steam gasification of Automotive Shredder residue; experiences from the Chalmers 2–4-MW indirect gasifier. Waste Manag. 102, 114–121. https://doi.org/10.1016/J.WASMAN.2019.10.037.
Marinho, A.L.A., Toniolo, F.S., Noronha, F.B., Epron, F., Duprez, D., Bion, N., 2021. Highly active and stable Ni dispersed on mesoporous CeO_2-Al_2O_3 catalysts for production of syngas by dry reforming of methane. Appl. Catal. B Environ. 281, 119459–119475. https://doi.org/10.1016/j.apcatb.2020.119459.
Moltó, J., López-Sánchez, B., Domene-López, D., Moreno, A.I., Font, R., Montalbán, M.G., 2020. Pollutant emissions during the pyrolysis and combustion of starch/poly(vinyl alcohol) biodegradable films. Chemosphere 256, 127107. https://doi.org/10.1016/j.chemosphere.2020.127107.
Nguyen, H.N.T., Seemann, M., Thunman, H., 2018. Fate of Polycyclic Aromatic Hydrocarbons during Tertiary Tar Formation in Steam Gasification of Biomass. Energy and Fuels 32 (3), 3499–3509. https://doi.org/10.1021/acs.energyfuels.7b0355810.1021/acs.energyfuels.7b03558.s001.
Palmer, D., Pou, J.O., Díaz-Ferrero, J., Conesa, J.A., Ortuño, N., 2021. Kinetics of the formation and destruction of PCDD/Fs in a laboratory tubular furnace. Chemosphere 276, 130175. https://doi.org/10.1016/j.chemosphere.2021.130175.
Qian, K., Kumar, A., 2017. Catalytic reforming of toluene and naphthalene (model tar) by char supported nickel catalyst. Fuel 187, 128–136. https://doi.org/10.1016/j.fuel.2016.09.043.
Quiroga, E., Cifuentes, B., Moltó, J., Ortuño, N., Conesa, J.A., Davó-Quiñonero, A., Cobo, M., 2021. Data of the integration of steam gasification and catalytic reforming of lignocellulosic biomass as a strategy to increase the syngas yield and pollutant removal - Mendeley Dataset. https://doi.org/10.17632/wsfzrnn5jw.2.
Quiroga, E., Moltó, J., Conesa, J.A., V alero, M.F., Cobo, M., 2020. Kinetics of the Catalytic Thermal Degradation of Sugarcane Residual Biomass Over Rh-Pt/CeO_2-SiO_2 for Syngas Production. Catalysts 10, 508–528. https://doi.org/10.3390/CATAL10050508.
Rathna, R., Varjani, S., Nakkeeran, E., 2018. Recent developments and prospects of dioxins and furans remediation. J. Environ. Manage. 223, 797–806. https://doi.org/10.1016/j.jenvman.2018.06.095.
Sahoo, D.R., Vajpai, S., Patel, S., Pant, K.K., 2007. Kinetic modeling of steam reforming of ethanol for the production of hydrogen over Co/Al_2O_3 catalyst. Chem. Eng. J. 125, 139–147. https://doi.org/10.1016/J.CEJ.2006.08.011.
Sanchez, N., Ruiz, R.Y., Cifuentes, B., Cobo, M., 2016. Hydrogen from glucose: A combined study of glucose fermentation, bioethanol purification, and catalytic steam reforming. Int. J. Hydrogen Energy 41 (13), 5640–5651. https://doi.org/10.1016/j.ijhydene.2016.01.155.
Savuto, E., Di Carlo, A., Gallucci, K., Natali, S., Bocci, E., 2017. Characterization and performance analysis of an innovative Ni/Mayenite catalyst for the steam reforming of raw syngas. Fuel 194, 348–356. https://doi.org/10.1016/j.fuel.2017.01.022.
Sehested, J., Carlsson, A., Janssens, T.V.W., Hansen, P.L., Datye, A.K., 2001. Sintering of nickel steam-reforming catalysts on MgAl2O4 spinel supports. J. Catal. 197 (1), 200–209. https://doi.org/10.1006/jcat.2000.3085.
Shayan, E., Zare, V., Mirzaee, I., 2018. Hydrogen production from biomass gasification; a theoretical comparison of using different gasification agents. Energy Convers. Manag. 159, 30–41. https://doi.org/10.1016/j.enconman.2017.12.096.
Aydin, E.S., Yucel, O., Sadikoglu, H., 2019. Experimental study on hydrogen-rich syngas production via gasification of pine cone particles and wood pellets in a fixed bed downdraft gasifier. Int. J. Hydrogen Energy 44 (32), 17389–17396.
Tan, R.S., Tuan Abdullah, T.A., Johari, A., Md Isa, K., 2020. Catalytic steam reforming of tar for enhancing hydrogen production from biomass gasification: a review. Front. Energy 14 (3), 545–569. https://doi.org/10.1007/s11708-020-0800-2.
Terrell, E., Theegala, C.S., 2019. Thermodynamic simulation of syngas production through combined biomass gasification and methane reformation. Sustain. Energy Fuels 3 (6), 1562–1572.

Tomishige, K., Miyazawa, T., Asadullah, M., Ito, S.I., Kunimori, K., 2003. Catalyst performance in reforming of tar derived from biomass over noble metal catalysts. Green Chem. 5, 399–403. https://doi.org/10.1039/b303371f.

Epa, U.S., 2018. Method 8270E Semivolatile Organic Compounds by GC/MS. U.S. EPA Test Methods SW-846. United States Environ. Prot. Agency.

Valderrama Rios, M.L., González, A.M., Lora, E.E.S., Almazán del Olmo, O.A., 2018. Reduction of tar generated during biomass gasification: A review. Biomass and Bioenergy 108, 345–370. https://doi.org/10.1016/j.biombioe.2017.12.002.

Vita, A., Italiano, C., Ashraf, M.A., Pino, L., Specchia, S., 2018. Syngas production by steam and oxy-steam reforming of biogas on monolith-supported CeO_2-based catalysts. Int. J. Hydrogen Energy 43 (26), 11731–11744.

Vita, A., Pino, L., Cipitì, F., Laganà, M., Recupero, V., 2014. Biogas as renewable raw material for syngas production by tri-reforming process over $NiCeO_2$ catalysts: Optimal operative condition and effect of nickel content. Fuel Process. Technol. 127, 47–58. https://doi.org/10.1016/j.fuproc.2014.06.014.

Weiland, F., Lundin, L., Celebi, M., van der Vlist, K., Moradian, F., 2021. Aspects of chemical recycling of complex plastic waste via the gasification route. Waste Manag. 126, 65–77. https://doi.org/10.1016/J.WASMAN.2021.02.054.

Wu, C., Williams, P.T., 2010. Pyrolysis-gasification of plastics, mixed plastics and real-world plastic waste with and without Ni-Mg-Al catalyst. Fuel 89 (10), 3022–3032. https://doi.org/10.1016/j.fuel.2010.05.032.

Wu, Y., Yang, W., Blasiak, W., 2014. Energy and exergy analysis of high temperature agent gasification of biomass. Energies 7, 2107–2122. https://doi.org/10.3390/en7042107.

Yan, M.i., Su, H., Zhou, Z., Hantoko, D., Liu, J., Wang, J., Wang, R., Kanchanatip, E., 2020. Gasification of effluent from food waste treatment process in sub- and supercritical water: H_2-rich syngas production and pollutants management. Sci. Total Environ. 730, 138517. https://doi.org/10.1016/j.scitotenv.2020.138517.

Yu, L., Song, M., Williams, P.T., Wei, Y., 2020. Optimized Reforming of Biomass Derived Gas Based on Thermodynamic and Kinetics Analysis with Activated Carbon Fibers Supported Ni-Al_2O_3. Bioenergy Res. 13 (2), 581–590. https://doi.org/10.1007/s12155-019-10087-6.

Zhang, L., Wu, W., Zhang, Y., Zhou, X., 2018a. Clean synthesis gas production from municipal solid waste via catalytic gasification and reforming technology. Catal. Today 318, 39–45. https://doi.org/10.1016/j.cattod.2018.02.050.

Zhang, R., Luo, Y., Yin, R., 2018b. Experimental study on dioxin formation in an MSW gasification-combustion process: An attempt for the simultaneous control of dioxins and nitrogen oxides. Waste Manag. 82, 292–301. https://doi.org/10.1016/J.WASMAN.2018.10.042.

Zhang, Z., Pang, S., 2019. Experimental investigation of tar formation and producer gas composition in biomass steam gasification in a 100 kW dual fluidised bed gasifier. Renew. Energy 132, 416–424. https://doi.org/10.1016/J.RENENE.2018.07.144.